Dissipative polarization domain walls in a passive driven Kerr resonator

Bruno Garbin,[1,2,3] Julien Fatome,[1,2,4] Gian-Luca Oppo,[5]
Miro Erkintalo,[1,2] Stuart G. Murdoch,[1,2] and Stéphane Coen[1,2,*]

[1] *Physics Department, The University of Auckland, Private Bag 92019, Auckland 1142, New Zealand*
[2] *The Dodd-Walls Centre for Photonic and Quantum Technologies, Dunedin, New Zealand*
[3] *Université Paris-Saclay, CNRS, Centre de Nanosciences et de Nanotechnologies, 91120, Palaiseau, France*
[4] *Laboratoire Interdisciplinaire Carnot de Bourgogne (ICB), UMR 6303 CNRS, Université de Bourgogne Franche-Comté, 9 Avenue Alain Savary, BP 47870, F-21078 Dijon, France*
[5] *SUPA and Department of Physics, University of Strathclyde, Glasgow G4 0NG, Scotland, European Union*

*** ABSTRACT COMING WITH THE NEXT ITERATION ***

Domain walls (DWs) are self-localized kink-type topological defects that connect two stable states of a physical system. They usually form in presence of a spontaneous symmetry breaking bifurcation [1], and are found in a variety of contexts, including magnetism [2], hydrodynamics [3], biology [4], Bose-Einstein condensates [5, 6], or string theory [7]. The paradigmatic examples are the interfaces that separate domains with distinct magnetization in ferromagnetic materials [2, 8, 9], whose unique properties are exploited in modern spintronics devices to store or even transfer information [10–12]. Additionally, DWs are central to numerous phase transitions in condensed matter and quantum physics [4, 13].

DWs are also known to manifest themselves in optical systems. In this context, the terminology was first used to describe stationary spatial distributions of light arising from the pure nonlinear (Kerr) interactions of counter-propagating beams [14] (and reported experimentally in [15]). Subsequently, Haelterman and Sheppard introduced the concept of DW *solitons* by describing vector, kink-type propagating structures, segregating homogeneous domains of orthogonal polarization states, and that resist diffractive or dispersive spreading in Kerr media [16]. Referred to as polarization DWs (or PDWs), these structures have only recently been convincingly observed experimentally by Gilles et al — more than two decades after their theoretical description — in the single-pass, *conservative*, propagation configuration of a normally dispersive single-mode optical fiber [17]. Remarkably, this experiment has demonstrated the potential of PDWs for transmission of topological bits, data robust to noise and fluctuations, as originally foreseen [18].

Here we extend the work of Gilles et al by implementing all-optical storage of PDWs. This is obtained by taking advantage of spontaneous symmetry breaking in an externally-driven passive resonator, enabling recirculation of PDWs [19]. Such *dissipative* PDWs have not been experimentally observed to date. It constitutes a key technology in supporting potential topologically-robust bit-based transmissions. By analogy, it would also enable for the real-time, stochastic, room temperature analog simulation of DW-related solid-state physics phenomena that would not be easily observable in other settings [20–22]. Finally, dissipative PDWs are also related to DWs predicted in the transverse structure of optical parametric oscillators (OPOs) [23, 24]. As the dynamics of these systems have been shown capable of estimating the ground state of the Ising Hamiltonian [25–27], associating domains of orthogonal polarizations segregated by dissipative PDWs with different spin states could provide a new route to solve complex optimization problems. We note that hints of dissipative PDWs "complexes" have been reported in fiber lasers, but these observations have proved hard to interpret [28–30]. In contrast, the results we present in this Letter provide the first clear signature of isolated dissipative temporal PDWs.

We start by describing theoretically the physics underlying the dissipative PDWs of our system. We consider a dispersive passive ring resonator that is externally, coherently driven by a continuous-wave (cw) light beam and that exhibits a Kerr nonlinearity. The resonator is supposed to be isotropic and the intracavity field is described in terms of the complex amplitudes, $E_{1,2}$, of the two orthogonal circular polarization components, which are assumed equally driven. In these conditions, the temporal evolution of the two modal amplitudes can be described by normalized coupled mean-field Lugiato-Lefever equations as [31, 32],

$$\frac{\partial E_{1,2}}{\partial t} = \Big[-1 + i\left(|E_{1,2}|^2 + B|E_{2,1}|^2 - \Delta\right) - i\frac{\partial^2}{\partial \tau^2}\Big] E_{1,2} + \sqrt{X/2}\,. \quad (1)$$

The terms of the right hand side of these equations describe respectively cavity losses, self- and cross-phase modulation, the cavity phase detuning, chromatic dispersion (assumed normal here, to avoid modulational in-

stabilities of cw stationary states of the resonator [32]), and external driving. t represents a slow time over which the evolution of the intracavity field takes place, at the scale of the cavity photon lifetime, while τ is a fast-time that allows to describe the temporal structure of the field along the round trip of the resonator. B is the cross-phase modulation coefficient ($B = 2$ for circularly polarized modes), Δ is the detuning parameter, which measures the separation between the driving laser frequency and the nearest cavity resonance in terms of the cavity half-linewidth, and X is the normalized total driving power.

Representative stationary ($\partial/\partial t = 0$) cw ($\partial/\partial\tau = 0$) solutions of the above equations are illustrated in Fig. 1(a). Because the equations are symmetric with respect to an interchange of the two polarization modes, $E_1 \rightleftarrows E_2$, the simplest stationary solutions express that symmetry ($E_1 = E_2$). This is in particular the case for the characteristics Kerr, S-shaped, bistable response that is plotted in Fig. 1(a) as a yellow curve. However, above a certain threshold of driving power, the upper-state solution undergoes a spontaneous symmetry breaking (SSB): the intensity of the two polarization modes part (blue and orange curves) [32–34]. Because of the symmetry of the system, there exists two such solutions, mirror-image of each other, in which a different mode dominates. These solutions correspond to intracavity fields that are overall elliptically polarized, with opposite handedness. This polarization SSB has been recently observed experimentally [35]. When the two symmetry-broken solutions are simultaneously excited in different regions (or domains) of the resonator, there exists a stationary temporal structure interconnecting them and across which the two polarization modes interchange: the PDW [Fig. 1(b)]. Note how the total intensity (grey curve) is nearly constant across the PDW. As shown numerically in [19], these dissipative PDWs can circulate indefinitely around a driven resonator without losing power or changing shape. Their robustness stems from a double balance, similar to that realized for bright temporal cavity solitons [36]: the external driving compensates the losses, while dispersive spreading is balanced by the nonlinearity. The latter occurs through the same mechanism as the conservative PDWs described by Haelterman and Sheppard [16].

The experimental setup that we have used to realize and control dissipative PDWs is depicted in Fig. 2. It is based on a $\simeq 10$ m-long passive optical fiber ring resonator mostly built out of highly nonlinear, normal dispersion, "spun" fiber, exhibiting very low birefringence due to twisting applied at the drawing stage [37]. The ring is closed with two SMF-28 fiber couplers, with splitting ratio 90/10 and 99/1, that enable respectively, injection of the driving and monitoring of the intracavity field. Overall the resonator exhibits normal dispersion at the 1550-nm driving wavelength, with averaged second order dispersion coefficient $\langle\beta_2\rangle \simeq 53$ ps^2/km and nonlinear coefficient $\langle\gamma\rangle \simeq 4.3$ W^{-1} km^{-1}. The free-spectral-range is found to be 19.8 MHz, corresponding to a round-trip time t_R of 50.6 ns. The measured finesse is about 24, amounting to losses of 26 % per round-trip, a photon lifetime of about $4\,t_R$, and a resonance width of 825 kHz.

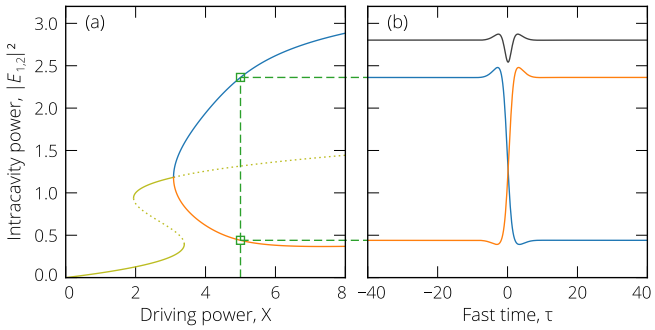

FIG. 1. Numerical illustration of the polarization SSB and associated PDWs for $\Delta = 3$ and $B = 2$ as described by Eqs. (1). (a) stationary cw solutions, $|E_1|^2$ and $|E_2|^2$, versus driving power X. The yellow curve represents symmetric solutions ($E_1 = E_2$; dotted lines are unstable states) while the blue and orange curves represent asymmetric solutions ($E_1 \neq E_2$). (b) Temporal intensity profile of a single PDW connecting the two cw symmetry-broken solutions existing for $X = 5$. Blue and orange curves correspond to the two polarization modes, while the black curve show total power.

The resonator is synchronously driven with flat-top 1.1 ns pulses. These pulses are obtained by carving the cw output of a 1 kHz linewidth, erbium-doped distributed-feedback fiber laser with a 10 GHz-bandwidth Mach-Zehnder amplitude modulator (AM). Pulse driving gives access to higher power levels, while also avoiding the detrimental effect of stimulated Brillouin scattering [38]. The AM modulator is followed by a fast polarization-modulator (PM) used to apply perturbations to the driving polarization as explained below. The two modulators are connected to separate pattern generators (PG) synchronized to the same $\simeq$ 10-GHz sinusoidal clock, set at a harmonic of the FSR. Before injection into the resonator, the driving pulses are amplified up to 15 W peak power (corresponding to X values up to 30) using an erbium-doped fiber amplifier (EDFA) combined with a band-pass filter (BPF) for rejection of amplified spontaneous emission noise. At the output, we monitor separately the power of the two polarization modes, split by a polarizing beam-splitter (PBS) preceded by a polarization controller (PC), as well as the total output power. These three signals are measured with a triplet of 10 Gb/s photodiodes. Additionally, a small fraction of the total output power is monitored and maintained constant by a PID feedback controller acting on the driving laser frequency, for stabilization of the detuning with respect to environmental fluctuations.

PDWs require interchange symmetry between the two polarization modes of the resonator. Our optical fiber

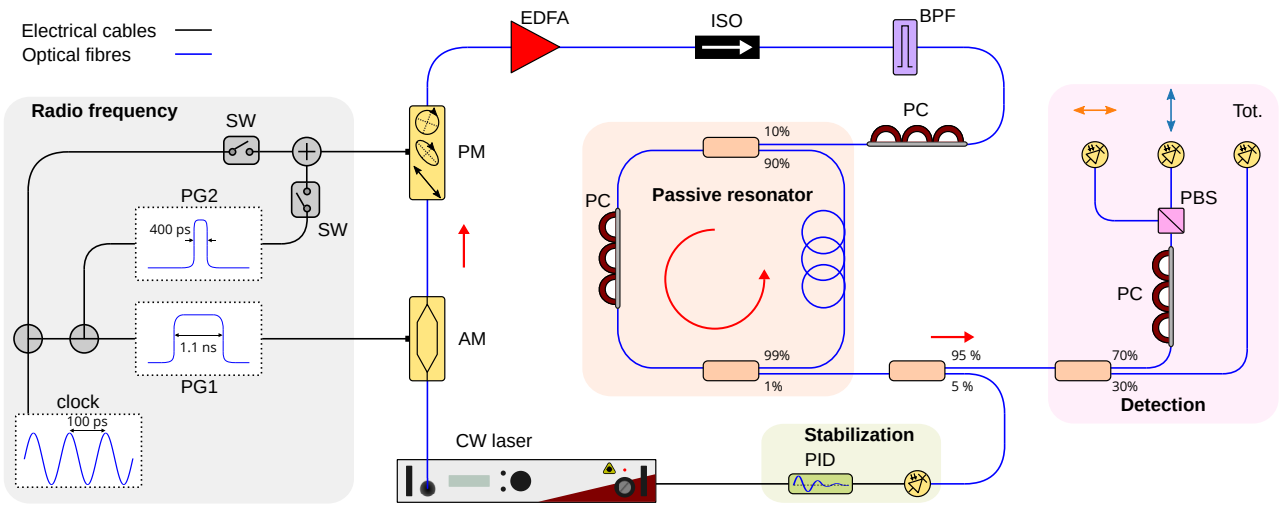

FIG. 2. Experimental set-up. The passive fiber ring resonator is highlighted with an orange background. CW laser, driving laser; AM, Mach-Zehnder amplitude modulator; PM, polarization modulator; clock, signal generator; PG1 and PG2, pattern generators; SW, electrical switch; EDFA, erbium-doped fibre amplifier; ISO, optical isolator; BPF, band-pass filter; PC, polarization controller; PBS, polarizing beamsplitter.

ring is however not completely isotropic. This is caused by the couplers, which are not built out of spun fiber, as well as unavoidable fiber bending. To counterbalance the residual cavity birefringence, a PC is incorporated into the fiber ring. In this configuration, the polarization modes are associated with states of polarization that typically evolve around the fiber ring, and that map onto themselves over one round-trip [39]. We can still identify these modes with the modal fields E_1 and E_2 in Eqs. (1). The cross-phase modulation coefficient B is reduced below 2 [17, 38], but PDWs exist so long as $B > 1$ [16]. Another PC, inserted before the input coupler, is used to project the driving field equally onto the two modes, and realize balanced driving conditions.

In practice, the system is tuned by observing the resonances of the two polarization modes of our resonator while scanning the driving laser frequency. A position of the intracavity PC is found for which, close to a point where the resonances overlap, their separation can be tuned without affecting their relative amplitudes. With the two resonances slightly apart, i) the output PC is set to correctly separate the modes in the detection stage, and ii) driving is balanced by matching the amplitudes of the observed resonances. Birefringence is then cancelled by superimposing the two resonances. Finally, we identify where the polarization SSB described in Fig. 1(a) (and reported in [35]) occurs by observing the cavity resonance while adjusting the driving power, and we lock the detuning within that region.

To proceed with observations of PDWs, we record the output power levels across our driving pulses over subsequent cavity round-trips using a 13-GHz-bandwidth real-time oscilloscope. A typical evolution is shown as color plots (bottom-to-top) in Figs. 3(a)–(c), with the three panels corresponding respectively to the powers of the two separate polarization modes and their total. Using matching colors, line plots are also presented in Fig. 3(d) for selected round trips. As can be seen, we start in a symmetry-broken state, where the "orange" mode uniformly dominates; see round trip #500 in panel (d). After about 1000 cavity round-trips, a localized, 400 ps-wide, RF perturbation is applied for about 20 round-trips to the PM, so as to carve a domain of different polarization in the middle of the driving pulse. We then let the intracavity field evolves freely for the rest of the measurement. Shortly after applying the perturbation, we observe at the output a sudden increase of the "blue mode" at a location corresponding to the perturbation, correlated with a depression of the "orange mode"; see round trip #1100 in panel (d). We now have a "domain" in which the blue mode dominates embedded within the original orange-dominated state. Everything appears as if the power levels of the two polarization modes have been interchanged in that domain, reflecting the mirror symmetry of the system. This symmetry can be further appreciated by noting that the color plots of the two polarization components measured throughout the experiment [Figs. 3(a) and (b)] are essentially negative images of each other. Correspondingly, the total output power [Fig. 3(c) and black curves in panel (d)] reveals little sign of the polarization structure of the intracavity field. We clearly are in presence of a pure polarization dynamics.

We identify the transition regions, along the fast-time (τ) coordinate, where the field switches polarization as two PDWs of opposite symmetry. The evolution shown in Fig. 3 reveals that these PDWs slowly drift towards each other (at a rate of about 0.15 ps/t_R); see also panel (e) where we plot the temporal separation between

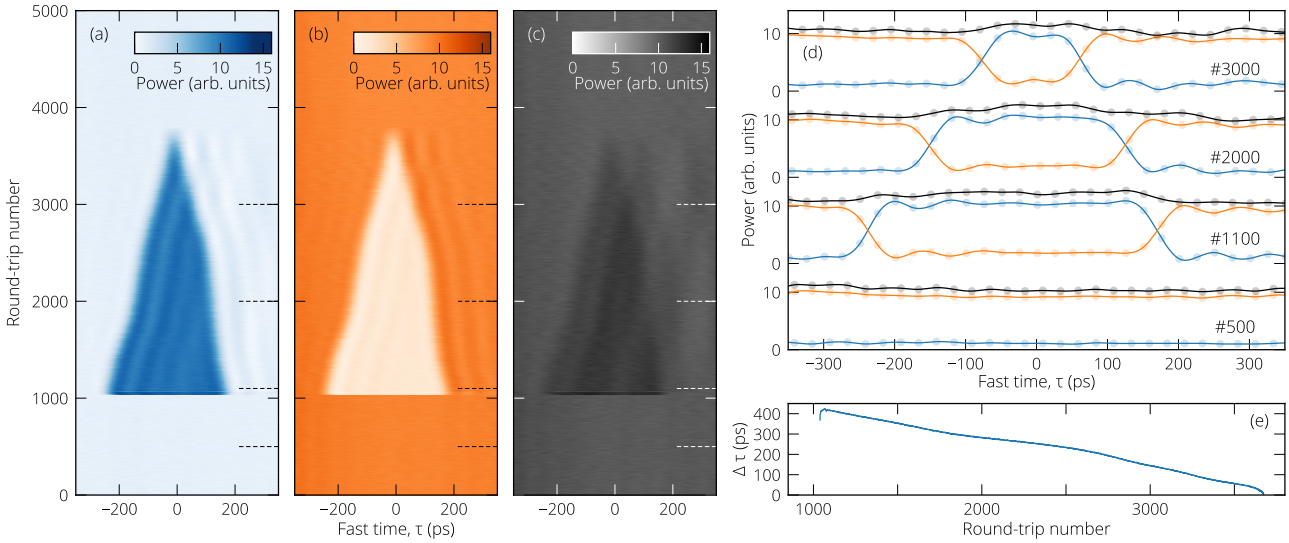

FIG. 3. Experimental evidence of dissipative PDWs, for $X \simeq 30.5$ and $\Delta \simeq 13.5$. (a)–(c) Round-trip-by-round-trip evolution of the fast-time output power profile for the two polarization components, $|E_{1,2}(\tau)|^2$ [(a), blue, and (b), orange] as well as for the total signal [(c), grey] before and after a short, localized, 400 ps-long polarization perturbation is applied at about round-trip #1000. The perturbation generates a "blue"-mode dominated domain connected to the surrounding regions by two PDWs. The PDWs drift towards each other, eventually mutually annihilating. (d) provides corresponding line plots using matching colors for selected round-trips as indicated (and marked as dashed side-lines in (a)–(c)]. (e) Evolution of the temporal separation between the PDWs.

the PDWs vs round-trip number. This results in the shrinkage of the blue-mode dominated domain created by the polarization perturbation. The PDWs eventually collide and mutually annihilate (around round trip #3800), reverting the system to its initial state. If the interchange symmetry between the polarization modes was perfect, the PDWs would have no preferred direction of motion and would remain still. We can therefore attribute the PDWs' motion to the presence of residual asymmetries, favoring one state over the other [35]. In particular, from the slight excess of total output power present in the central domain, we can infer that the blue mode may have been driven a little bit stronger than the orange mode. Nevertheless, the PDWs are very robust: they persist for nearly one thousand photon lifetime while maintaining their stiffness (as far as the 80 ps temporal resolution of our real-time oscilloscope allows to judge), demonstrating their dissipative and nonlinearly-localized character.

In order to observe PDWs in stationary conditions, we have investigated the use of an external modulation of parameters to trap PDWs, as that technique has been successfully exploited to pin various types of moving fronts in other nonlinear systems [40–45]. In our case, we modulate the polarization of the driving field, by applying a small fraction of the 10 GHz sinusoidal clock signal to the PM (see Fig. 2). This modulation can be turned on and off with an additional rf switch (SW). Figure 4(a) shows the result of an experiment that starts like that discussed in Fig. 3 (only showing one polarization component), with two PDWs initially drifting towards each other at a constant speed. Upon application of the modulation from round-trip #1200 [the modulation is plotted in Fig. 4(b) as well as overlaid to the data in panel (a) with transparent shades of red], we immediately observe a change of behavior. The PDWs visibly change speed and, after some transient, eventually reach a fixed position with respect to the modulation. That position is such that the local driving imbalance imparted by the modulation confers to the PDWs a drifting speed that counteracts the original motion induced by the other asymmetries [35]. The PDWs hold their position until the modulation is turned off at round-trip #2500, which releases them and puts them back on their original collision course. In Fig. 4(c), using the same technique, we demonstrate long term pinning of two PDWs over 30 seconds (corresponding to a propagation distance of 6×10^6 km inside the resonator), which has enabled us to measure their temporal intensity profile with a 65-GHz sampling oscilloscope [blue dots in Fig. 4(d)]. While this measurement is still bandwidth limited, it demonstrates that the PDWs have a rise time of less than 10 ps, to be compared to the 2.5 ps numerical expectation [green curves in Fig. 4(d)].

We remark that the PDWs reported in Figs. 3 and 4 are observed for driving powers comparatively larger than that considered in the theoretical plot of Fig. 1. Large driving powers are made necessary by the presence of linear coupling between the polarization modes of our fiber resonator [caused in part by fiber bending, and not included in Eqs. (1)]. Numerical calculations indicate that

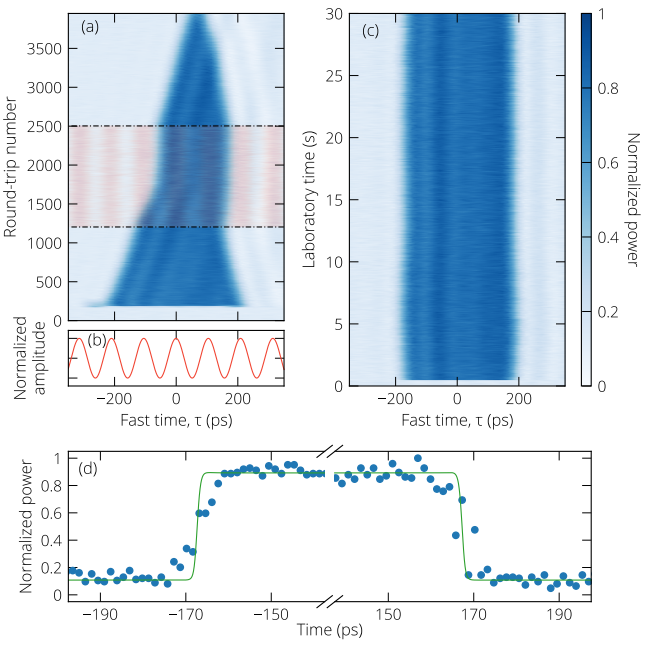

FIG. 4. (a) Demonstration of drifting PDWs being pinned/unpinned to a shallow modulation of the driving polarization. We only show the evolution of the output power of one polarization component. The 10 GHz sinusoidal modulation [transparent shades of red and panel (b)] is applied between round-trips #1200 and 2500. (c) Long term pinning of PDWs, for $X \simeq 24$ and $\Delta \simeq 9.2$. (d) Sampling scope measurement (blue dots) of the temporal intensity profile of the two PDWs trapped in (c). The green curve is the numerical expectation.

linear coupling, which splits the cavity resonance [46], thwarts polarization SSB at low power. SSB and PDWs are restored at high power, when the Kerr-induced tilt of the cavity resonance dominates over the splitting [47].

In conclusion, we have reported here the first experimental demonstration of dissipative PDWs. The PDWs are recirculated in a passive, driven Kerr optical fiber ring resonator. Their existence relies on a symmetry breaking bifurcation and on an interchange symmetry between the two polarization modes of the resonator. Our dissipative PDWs are found to be robust with respect to residual imperfections and asymmetries, and can be pinned to a shallow external modulation. Given their duration, our resonator could hold up to 20,000 PDWs in a cw-driven configuration. Our results suggest that our system could be used as an all-optical buffer for PDW-based topological bit transmissions [17]. Optical PDWs could also prove useful for the real time stochastic analog simulation of other DW-related phenomena.

* s.coen@auckland.ac.nz

[1] M. Golubitsky, I. Stewart, and D. G. Schaeffer, *Singularities and Groups in Bifurcation Theory: Volume II*, Applied Mathematical Sciences No. 69 (Springer-Verlag, New York, 1988).
[2] P.-E. Weiss, J. Phys. Theor. Appl. **6**, 661 (1907).
[3] F. Tsitoura, U. Gietz, A. Chabchoub, and N. Hoffmann, Phys. Rev. Lett. **120**, 224102 (2018).
[4] L. E. Reichl, *A Modern Course in Statistical Physics*, 4th ed. (Wiley-VCH, 2016).
[5] S. Coen and M. Haelterman, Phys. Rev. Lett. **87**, 140401 (2001).
[6] D. M. Stamper-Kurn and M. Ueda, Rev. Mod. Phys. **85**, 1191 (2013).
[7] S. Weinberg, *The Quantum Theory of Fields*, Vol. 2 (Cambridge University Press, 1995).
[8] D. Y. Parpia, B. K. Tanner, and D. G. Lord, Nature **303**, 684 (1983).
[9] J. Unguris, R. J. Celotta, and D. T. Pierce, Phys. Rev. Lett. **67**, 140 (1991).
[10] D. A. Allwood, G. Xiong, C. C. Faulkner, D. Atkinson, D. Petit, and R. P. Cowburn, Science **309**, 1688 (2005).
[11] S. S. P. Parkin, M. Hayashi, and L. Thomas, Science **320**, 190 (2008).
[12] J. A. Currivan-Incorvia, S. Siddiqui, S. Dutta, E. R. Evarts, J. Zhang, D. Bono, C. A. Ross, and M. A. Baldo, Nat. Commun. **7**, 10275 (2016).
[13] A. Dutta, G. Aeppli, B. K. Chakrabarti, U. Divakaran, T. F. Rosenbaum, and D. Sen, *Quantum Phase Transitions in Transverse Field Spin Models: From Statistical Physics to Quantum Information* (Cambridge University Press, Cambridge, 2015).
[14] V. E. Zakharov and A. V. Mikhailov, JETP Lett. **45**, 349 (1987).
[15] S. Pitois, G. Millot, and S. Wabnitz, Phys. Rev. Lett. **81**, 1409 (1998).
[16] M. Haelterman and A. P. Sheppard, Opt. Lett. **19**, 96 (1994); A. P. Sheppard and M. Haelterman, *ibid.* **19**, 859 (1994).
[17] M. Gilles, P.-Y. Bony, J. Garnier, A. Picozzi, M. Guasoni, and J. Fatome, Nature Photon. **11**, 102 (2017).
[18] M. Haelterman, Electron. Lett. **30**, 1510 (1994); M. Haelterman and M. Badolo, Opt. Lett. **20**, 2285 (1995).
[19] J. Fatome, F. Leo, M. Guasoni, B. Kibler, M. Erkintalo, and S. Coen, in *Nonlinear Photonics, NP'2016* (Optical Society of America, Sydney, NSW, Australia, 2016) p. NW3B.6.
[20] G.-L. Oppo, A. J. Scroggie, and W. J. Firth, Phys. Rev. E **63**, 066209 (2001).
[21] D. V. Skryabin, A. Yulin, D. Michaelis, W. J. Firth, G.-L. Oppo, U. Peschel, and F. Lederer, Phys. Rev. E **64**, 056618 (2001).
[22] I. Rabbiosi, A. J. Scroggie, and G.-L. Oppo, Phys. Rev. Lett. **89**, 254102 (2002).
[23] S. Trillo, M. Haelterman, and A. Sheppard, Opt. Lett. **22**, 970 (1997).
[24] G.-L. Oppo, A. J. Scroggie, and W. J. Firth, J. Opt. B: Quantum Semiclass. Opt. **1**, 133 (1999).
[25] Z. Wang, A. Marandi, K. Wen, R. L. Byer, and Y. Yamamoto, Phys. Rev. A **88**, 063853 (2013).
[26] A. Marandi, Z. Wang, K. Takata, R. L. Byer, and Y. Yamamoto, Nature Photon. **8**, 937 (2014).
[27] T. Inagaki, Y. Haribara, K. Igarashi, T. Sonobe, S. Tamate, T. Honjo, A. Marandi, P. L. McMahon, T. Umeki, K. Enbutsu, O. Tadanaga, H. Takenouchi, K. Aihara,

K.-i. Kawarabayashi, K. Inoue, S. Utsunomiya, and H. Takesue, Science **354**, 603 (2016).
[28] Q. L. Williams, J. García-Ojalvo, and R. Roy, Phys. Rev. A **55**, 2376 (1997).
[29] H. Zhang, D. Y. Tang, L. M. Zhao, and X. Wu, Phys. Rev. B **80**, 052302 (2009).
[30] C. Lecaplain, P. Grelu, and S. Wabnitz, J. Opt. Soc. Am. B **30**, 211 (2013).
[31] L. A. Lugiato and R. Lefever, Phys. Rev. Lett. **58**, 2209 (1987).
[32] M. Haelterman, S. Trillo, and S. Wabnitz, J. Opt. Soc. Am. B **11**, 446 (1994).
[33] A. E. Kaplan and P. Meystre, Opt. Commun. **40**, 229 (1982).
[34] I. P. Areshev, T. A. Murina, N. N. Rosanov, and V. K. Subashiev, Opt. Commun. **47**, 414 (1983).
[35] B. Garbin, J. Fatome, G.-L. Oppo, M. Erkintalo, S. G. Murdoch, and S. Coen, *Asymmetric Balance in Symmetry Breaking*, arXiv 1904.07222 [nlin, physics:physics] (2019) arXiv:1904.07222.
[36] F. Leo, S. Coen, P. Kockaert, S.-P. Gorza, Ph. Emplit, and M. Haelterman, Nature Photon. **4**, 471 (2010).
[37] A. J. Barlow, J. J. Ramskov-Hansen, and D. N. Payne, Appl. Opt. **20**, 2962 (1981).
[38] G. P. Agrawal, *Nonlinear Fiber Optics*, 5th ed. (Academic Press, 2013).
[39] S. Coen, M. Haelterman, Ph. Emplit, L. Delage, L. M. Simohamed, and F. Reynaud, J. Opt. Soc. Am. B **15**, 2283 (1998).
[40] N. N. Rozanov, V. E. Semenov, and G. V. Khodova, Sov. J. Quantum. Electron. **12**, 193 (1982), translated from Kvantovaya Elektron. (Moscow) 9, 354-360 (Feb. 1982).
[41] Y. Pomeau, Physica D **23**, 3 (1986).
[42] S. Coen, M. Tlidi, Ph. Emplit, and M. Haelterman, Phys. Rev. Lett. **83**, 2328 (1999).
[43] F. Haudin, R. G. Elías, R. G. Rojas, U. Bortolozzo, M. G. Clerc, and S. Residori, Phys. Rev. E **81**, 056203 (2010).
[44] F. Marino, G. Giacomelli, and S. Barland, Phys. Rev. Lett. **112**, 103901 (2014).
[45] J. K. Jang, M. Erkintalo, S. Coen, and S. G. Murdoch, Nature Commun. **6**, 7370 (2015).
[46] J. R. Pierce, J. Appl. Phys. **25**, 179 (1954).
[47] L. Del Bino, J. M. Silver, S. L. Stebbings, and P. Del'Haye, Sci. Rep. **7**, 43142 (2017).